Unveiling the layers of history: a hybrid profiling approach for the characterisation of heritage objects

M. DINU*, L. GHERVASE, L. C. RATOIU, I. M. CORTEA, L. M. ANGHELUTA, A. M. PATRASCU, C. M. STANCU, V. A. CRISTEA
National Institute of Research and Development for Optoelectronics INOE 2000, Măgurele, Ilfov, 077125, Romania

This article presents an innovative analytical setup that integrates advanced optoelectronic methods: hyperspectral imaging, Raman spectroscopy, and Laser-Induced Breakdown Spectroscopy (LIBS) to create a comprehensive real-time "profile" of heritage objects. By leveraging macroscopic hyperspectral imaging for initial material identification and pixel-by-pixel analysis for detailed composition, the hybrid setup proceeds to micron-level insights through Raman spectroscopy, culminating in stratigraphic data from LIBS. The novel "profiler" method synchronizes these complementary techniques, enabling the collection of a rich, layered dataset that correlates spectral data to precise material depths for each LIBS pulse.

1. Introduction

The study and preservation of cultural heritage have increasingly become interdisciplinary endeavours, incorporating insights from chemistry, physics, and materials science. Recent advancements in optoelectronic techniques have transformed the way researchers understand heritage objects, enabling unprecedented exploration of their physical and chemical properties. Among these techniques, hyperspectral imaging, Raman spectroscopy, and Laser-Induced Breakdown Spectroscopy (LIBS) stand out for their complementary abilities to provide detailed insights into the composition and degradation mechanisms of artefacts.

Hyperspectral imaging (HSI) is a non-invasive technique that captures a broad spectrum of light across numerous wavelengths, allowing for the identification of materials based on their unique spectral signatures. This method has been successfully applied in the analysis of paintings, textiles, manuscripts and archaeological artefacts and has proven effective in identifying pigments and binding media. Its macroscopic imaging capabilities allow researchers to conduct preliminary surveys, identify areas of interest, and target for more detailed examination [1-5].

Raman spectroscopy, characterized by its capability to analyse molecular vibrations, offers micro-scale insights into the composition of heritage objects. This technique provides information about molecular bonding and chemical structures and is valuable for identifying different types of materials encountered in the field of cultural heritage, such as organic compounds, pigments, binders or minerals. The non-destructive nature of Raman spectroscopy makes it particularly suited for studying fragile artefacts, ensuring the preservation of their integrity during examination [6-12].

On the other hand, LIBS provides elemental analysis through the excitation of materials with a laser pulse, generating a plasma that emits light characteristic of the elements present. This technique has been adapted for depth profiling, enabling researchers to gather stratigraphic data from the surface to the subsurface of materials. This feature is particularly useful for understanding the layered construction of artefacts, shedding light on their historical and material complexities [13-20].

The integration of these optoelectronic techniques offers a multifaceted view of heritage objects, facilitating therefore a more comprehensive understanding. By combining the broad material identification capabilities of hyperspectral imaging, the molecular-level insights of Raman spectroscopy, and the depth profiling abilities of LIBS, researchers can develop a robust analytical framework that informs both academic study and conservation strategies. This article presents an optoelectronic setup that integrates these techniques into a cohesive profiling system, with the potential to significantly advance the field of heritage science.

2. State of the art

In recent years, the demand for advanced analytical techniques has grown significantly across various sectors including environmental science, art conservation, and healthcare. HSI, LIBS, and Raman spectroscopy are three optoelectronic techniques that, when combined, offer comprehensive insights into the composition and properties of various materials. Each technique offers unique strengths; HSI provides spatial information, LIBS allows for stratigraphic elemental analysis, and Raman spectroscopy offers molecular-level insights.

The use of LIBS in Cultural Heritage has attracted attention for many years, in part due to the ability for *in-*

situ, rapid, minimally destructive, multi-element analysis, depth-profiling, and compatibility with other techniques such as Raman spectroscopy. There are several reviews that have focused specifically on laser spectroscopy techniques in art, archaeology, and cultural heritage [21-24].

LIBS and Raman spectroscopy techniques utilize similar equipment for spectra induction and detection. Generally, in a Raman instrument, continuous-wave lasers can be effectively employed if extraneous emissions (e.g., sunlight, room lighting, etc.) are comparatively weak or somehow attenuated by the instrument casing. Nanosecond or picosecond lasers are becoming increasingly popular in literature due to perspectives for unique remote sensing applications or depth profiling measurements [25-30] [25-30]. The instrumental development followed a logical trend: first, separate instruments were used, then hybrid units were developed consisting of single laser and a single detector, and more recently new laser types and spectrometers have been implemented in the combination [31-33]. Giakoumaki et al. created a hybrid unit aimed at examining of cultural heritage samples and objects, employing a single laser operating at 532 nm and capturing spectra with a non-intensified CCD [34]. Additionally, Marquardt et al. developed a fibre optic probe system for conducting Laser-Induced Breakdown Spectroscopy (LIBS), Raman point analysis, and Raman imaging of particles on soil substrates, utilizing different lasers to generate both the plasma and the Raman signals [35]. There are studies focused on analysing biogenic and inorganic minerals using a standoff configuration with a single laser system, where the Raman excitation was achieved through a frequency-doubling crystal positioned before the LIBS laser, alongside a super-notch filter placed in the detector's pathway [36,37]. Subsequently, Hoehse et al. introduced a two-laser LIBS-Raman micro-analysis system featuring a dual-arm high-resolution Echelle spectrometer and a single non-intensified CCD that performs similar to advanced Raman scanning microscopes, although LIBS achieves detection limits in the parts per million (ppm) range and offers extensive spectral coverage from 290 to 945 nm [38]. The synergistic benefits of LIBS and Raman techniques correlation are demonstrated [39]. At this time, there are multiple strategies for integrating Raman-LIBS technologies into a single instrument. These strategies include using either two distinct laser sources or a single laser with adjustable output pulse energy, potentially incorporating time/space differentiation. Various optoelectronic systems have been employed across a wide range of applications, including chemical mapping, ESA missions, remote detection of explosives, depth profiling, food authentication and the study of cultural heritage artefacts [40-50]. A variety of visible and near-infrared hyperspectral imaging (Vis-NIR HSI) systems provide significant flexibility and multiple options for inspecting diverse materials. Depending on the configuration of the illumination system relative to the optical detector, HSI typically operates in three sensing modes: reflectance, transmittance, and interactance [51-55]. HSI analysis generates a synergistic effect that allows for a thorough characterization of unknown samples. Laser-Induced Breakdown Spectroscopy (LIBS) is a fast, multi-element analytical method that excels in quantifying both light and heavy elements [25-26]. However, it falls short in identifying polymorphs or distinguishing between mixtures of crystals. In contrast, Raman spectroscopy can effectively differentiate between polymorphs due to variations in their crystal structures. Nonetheless, interpreting Raman spectra can be complex, particularly when analysing natural mineral mixtures. In these instances, understanding the elemental composition can greatly facilitate the interpretation of Raman spectra [49]. While each technique individually yields valuable but limited results, the development of a single instrument that integrates Raman, LIBS and HSI techniques offers real-time, comprehensive data - without the need for sampling or sample preparation [18,39,57-65].

3. Experimental setup

Raman spectroscopy and Laser Induced Breakdown Spectroscopy (LIBS) are two complementary techniques frequently used in modern analytical chemistry applications because of their unique feature for express analysis of any sample type in any environment. Both methods are based on laser light-matter interaction, which results in scattered/induced optical emission providing information on the sample composition. Raman spectroscopy is a powerful tool for express molecular analysis based on inelastic scattering of pumping laser photons by molecular/crystal vibration. LIBS provides both quantitative and qualitative multi-elemental analysis by inducing ablation and atomization of the sample with subsequent quantification of the laser-induced atomic/ionic emission spectrum. The remarkable feature of both Raman and LIBS measurements is the remote analysis capability when target must be "only photon reachable". For example, LIBS analysis requires only laser photons to induce laser plasma and only photons to collect plasma emission. Hyperspectral analysis offers both imaging and spectral data, measuring the spatial information and the spectral parameters for each pixel, simultaneously. The hyperspectral image is expressed as a hypercube $I(x, y, \lambda)$, containing wavelength λ and spatial (x, y) dimensions. The results of the hyperspectral analysis can be used either as a spectral data $I(\lambda)$ for each individual pixel (x, y), or as an image $I(x, y)$ for each wavelength λ [54]. Each pixel is attributed a unique spectral fingerprint, which can be used to characterize its chemical composition. As such, hyperspectral imaging can be used for the identification and quantification of chemical compositions, and in the same time for mapping their distribution [66-67].

The optomechanical scheme for correlation of LIBS (C1) with Raman (C2) and HSI (HS) is outlined in Fig. 1, and contains a pulsed YAG:Nd laser with a frequency doubler crystal for 2nd harmonic generation (532 nm), 20 ns pulse duration, variable frequency of 1-20 Hz as the excitation source (L), a pulse generator (T_g), an Echelle-type spectrometer with a spectral range of 180-780 nm coupled with an ICCD (S), optical fibres for collecting and

transmitting (F_o) and specific lenses and filters for LIBS and Raman. The fundamental wavelength is blocked using a filter in order to prevent sample heating. A conventional backscattering optical scheme is used both for Raman and LIBS analyses. The laser beam is focused on the surface of

the cultural heritage objects using quartz lenses. The same lens captures the backscattered radiation, which is guided by a pierced mirror through a holographic Notch filter (L_r) and a second focusing lens to the optical collector.
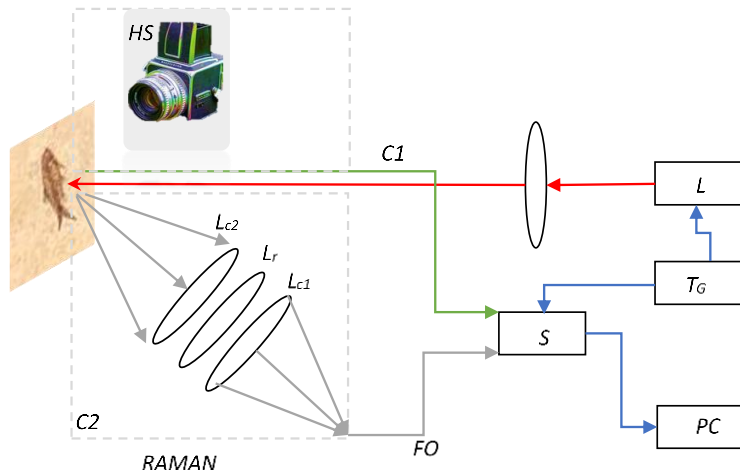

Fig. 1. LIBS-RAMAN-HSI experimental setup (color online)

The hyperspectral camera (HS) is triggered first and provides a distribution map of the materials/elements present that helps select in real-time the interest areas that require further detailed analyses. The laser system is then aligned to the position(s) selected by the hyperspectral preliminary imagistic analysis and triggered accurately. The laser emits first a low energy laser pulse with fluency below the damage threshold - specific for the Raman measurements and secondly a laser pulse with a higher energy and a fluency sufficient to sustain a plasma plume - for LIBS measurements. The signal is collected using an optical collector and transmitted through optical fibres to the spectrometer. An Echelle-type spectrometer was chosen because it is suitable for both LIBS and Raman. The acquisition of the spectral data is made on single pulse mode for the LIBS data, and on Raman shift for the Raman data. Depending on the type of the material depicted preliminary by the hyperspectral (polychrome or not, multilayer or not), the laser can be triggered once (for simple materials) or in succession of pulses for stratigraphy LIBS and Raman (polychrome, multilayer materials, corrosion affected objects etc.).

4. Results and discussions

The hybrid setup integrates the three complementary techniques, producing a robust data package that correlates hyperspectral, Raman, and qualitative LIBS data with the precise depth of material ablation for each LIBS pulse. The key advantage of the method is its capability to create a real-time profile of the investigated heritage object as the analysis progresses. Each LIBS pulse generates data that are immediately linked to the concurrent hyperspectral and Raman analyses, enabling a comprehensive understanding

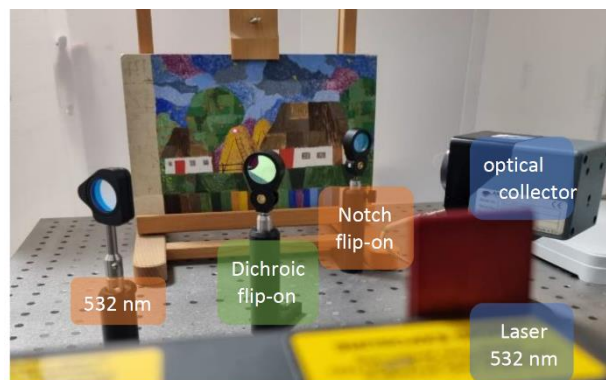of the object's condition at both macroscopic and microscopic levels.

Fig. 2. LIBS-RAMAN lab setup (color online)

This dynamic interplay between techniques results in a rich, layered dataset that provides insights into the historical and material complexities of the object under investigation. With LIBS adding the stratigraphic component to the analysis, contouring a structured interpretation of the materials, it tracks down how different layers may have been affected by environmental changes or restoration interventions, offering a temporal context that is often missing from traditional analytical techniques.

At the macroscopic level, hyperspectral imaging captures a wide range of wavelengths from the electromagnetic spectrum, creating a detailed 2D representation of the target object. Each pixel in the image corresponds to a specific spectral signature, allowing researchers to identify and differentiate materials based on their unique absorption and reflectance properties. This

initial imaging step serves as the foundation for further analysis, providing a broad overview of the object's material composition. This step is crucial for discriminating pigments, binders, or any other significant materials that may differ. It establishes a baseline understanding of the object's condition and composition. Raman spectroscopy complements the hyperspectral data by providing information at molecular-level, particularly useful for identifying organic compounds and characterizing complex mixtures. By focusing on specific areas of interest identified through hyperspectral imaging, this micron-level analysis allows for a deeper understanding of the materials, offering valuable insights into degradation processes or historical alterations. LIBS takes the analysis a step further by providing stratigraphic information by advancing pulse-by-pulse into the layers of material. LIBS generates a 3D profile of the object's composition, revealing variations in elemental content across different layers.

A series of analyses and tests were carried out to validate the functionality of the components of the hybrid system, starting from simpler casuistic (*a.-c.*) and concluding in a case study on polychrome multi-layered samples (*d.*).

4.1. Bricks and mortars

One of the studies was aimed at discriminating the original bricks and mortars from the Turkish Bath from Golești Museum, Romania, given that during the restoration new bricks were also used, next to the original fragments. Since the properties of medieval and modern bricks vary in what regarding the raw materials, the production methodology, as well as the mortars used, imagistic and spectroscopic methods were combined in order to analyse, assess the state of conservation, and map the original elements, as well as document the previously performed interventions.
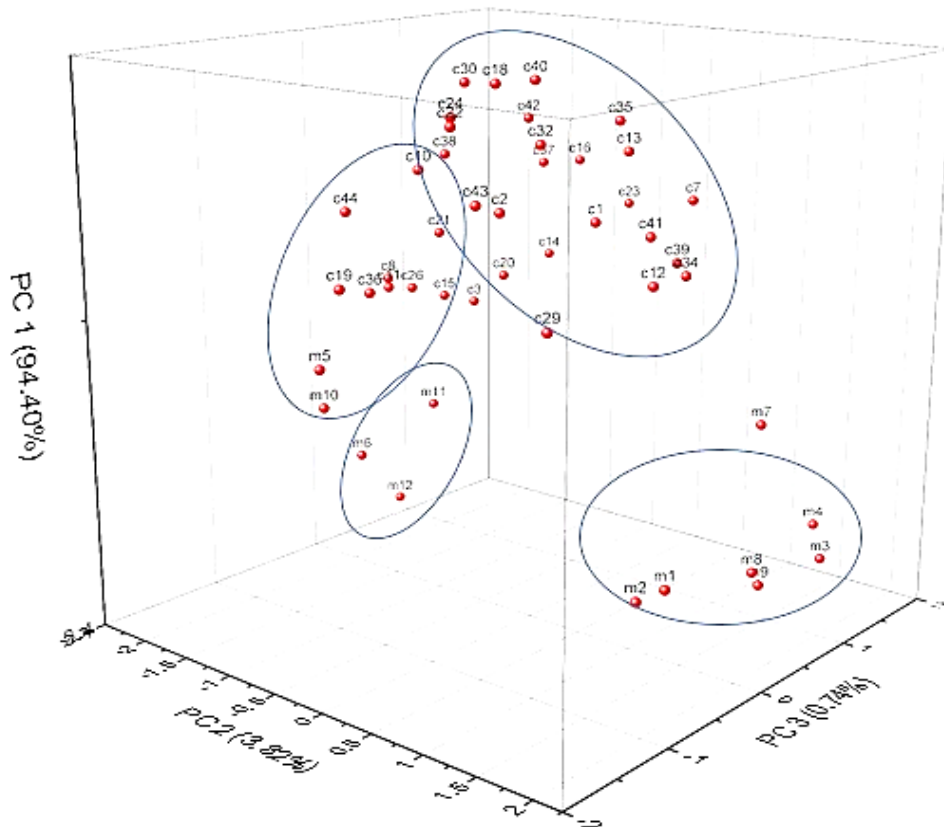

Fig. 3. PCA applied to bricks (c) and mortars (m) [68] (color online)

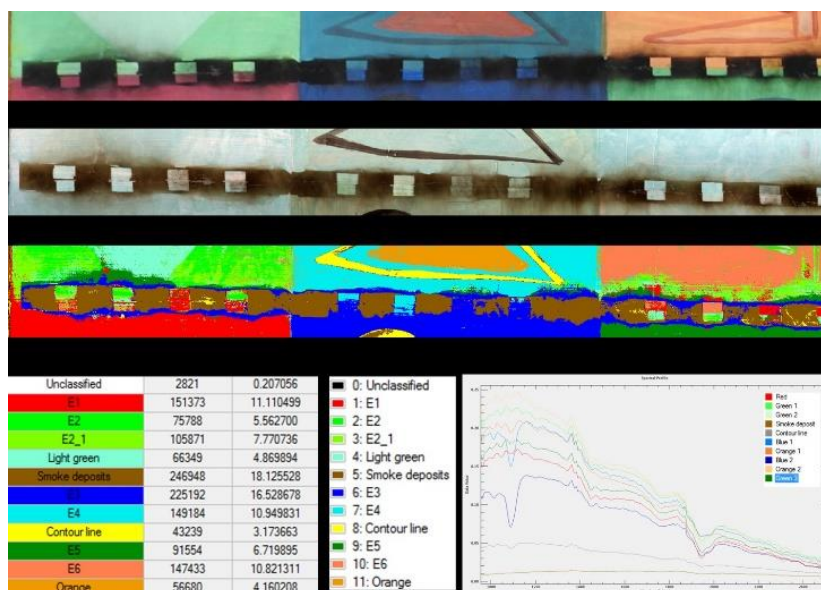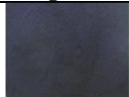*Fig. 4. SAM Classification (color online)*

The main chemical constituents of clay are silicon (Si) and aluminium (Al), but also a number of minor elements and trace elements that were used in the analysis multivariate data. Thus, the imagistic data (HSI) were corroborated with the spectroscopic data (atomic and molecular) resulting in a map of the original bricks and mortars. The Spectral Angle Mapper (SAM) classification is presented in Fig. 3 [68].

Principal Component Analysis (PCA) was applied on the LIBS data aiding the classification and discrimination of the original materials from the recent ones. All the chemical elements detected were used in the analysis, as they can influence the discrimination and the complete matrix must be taken into consideration. PCA helped distinguish between two types of bricks and mortar, as it can be observed in Fig. 4 [68].

4.2. Mural paintings

The investigated artwork is part of a set of murals created by a contemporary artist using modern pigments, in *a secco* and *buon* fresco painting techniques. The pigment particles are mixed in water and applied to a layer of fresh lime, and, due to the carbonation process by which the pigments are fixed in the support, the spectral variability of the spectral profile is reduced, with most pigments showing very similar LIBS spectra. For this reason, the characterization requires a complex approach involving the corroboration of data obtained by complementary techniques: LIBS and hyperspectral analysis. The data obtained by supervised classification, corroborated with LIBS elemental analysis, resulted in a distribution map that allowed the laser cleaning to be tracked accordingly to each area specificity [69].

Fig. 5. Hyperspectral data classification (color online)

4.3. Archaeological objects

This casuistic is focused on the discrimination of metal archaeological objects from Hallstatt, which are typologically similar (in general terms), using multivariate analysis of spectral data obtained by LIBS and RAMAN spectroscopy. LIBS was used in single pulse configuration for stratigraphic analysis (10-100 series) and RAMAN was correlated for obtaining a detailed classification of the objects extracted by archaeological excavation (or from other random discoveries) based on the elemental composition of the original material.

Fig. 6. PCA classification (color online)

The obtained spectral data were processed using advanced statistical analysis methods and then clustered by similarities, thus obtaining a detailed classification of objects recovered from archaeological excavations (or from other random finds) based on the elemental composition of the original material, as observed in Fig. 6. The PCA analysis helped to determine the corrosion layers and discriminate based on their thickness, as the first 20 pulses reveal a greater inhomogeneity. based on the preliminary results, the red group can be correlated to a different site; the blue group are bronze rings with similar composition that based on the PCA can be attributed to the same necklace; the grey group are related.

4.4. Case study on polychrome multi-layered samples

To simulate complex cases similar to those encountered in the cultural heritage field, experimental models were created using historical painting techniques and traditional pigments. This approach provides a valuable information base on the varied behaviour of colour mixtures used by artists throughout the history of painting. Thus, the choice of painting materials as well as the techniques selected for the realization of the experimental models followed a methodological plan that, through complementary analyses, would allow highlighting the behaviour of certain pigments mixed with various binders. The mock-ups comprise different pigments and binders applied on a support made of coated cardboard (produced by Phoenix Arts Group). The pigments used are from Schmincke. This resulted in complex models with multiple variables. All the materials used to make these samples are summarized in Table 1.

Table 1. Pigments used for the mock-up

Pigment	Chemical formula	Toxicity	Image
Prussian blue (Paris blue)	$Fe_4[Fe (CN)_6]_3$ $n = 1.56-1.662$	Moderate	
vermilion	HgS $n = 2.905-3.256$	Yes	
red iron oxide (English red)	Fe_2O_3 $n = 2.78–3.01$	No	
Bohemian green (earth green)	$(K,Na)(Fe^3,Al,Mg)_2 (Si,Al)_4O_{10}(OH)_2$ $n = 1.62$	No	
black iron oxide	Fe_3O_4 $n = 2.42$	No	
smoke black (lamp black)	C opaque	No	
charcoal black	C_{60} si C_{70} opaque	No	
ivory black (bone black)	$Ca_5(OH)(PO_4)_3 + C$ $n = 1.65-1.70$	No	
graphite	C opaque	No	

The canvas is made exclusively of cotton, and gesso has been applied in three successive layers to provide a preparation layer with the smoothest texture. Afterwards, there were added the charcoal preparatory drawing and paint layers of four different colours, selected precisely for

the different refractive index (n): Prussian blue, vermilion, iron red, green earth. Egg yolk, egg white, linseed oil, casein, tempera grassa (a mixture of linseed oil, white wine and egg yolk) were used as binders. Each sample was divided into 5 columns and 5 rows: row I comprises the pattern with egg yolk emulsion as dispersion medium, repeated over 5 columns; row II includes the pattern with

egg white, repeated on the 5 columns; row III includes the pattern with linseed oil, repeated on all 5 columns; row IV contains the pattern with casein, repeated on all columns and row V includes the pattern with tempera grassa was used as a dispersion medium, according to the previously mentioned recipe, repeated on the 5 columns, as can be observed in Fig. 7.

Fig. 7. Mock-up: a. pigments, b. adding the black layers (color online)

Afterwards, 3 successive layers of black mixed with fat tempera or casein were applied, using black iron oxide on column 1, smoke black on 2, carbon black on 3, black ivory on 4, and graphite on column 5. Covering the initial base with black pigments was done gradually, in three sequences (respecting the way of application of the colours and the drying time), using the same proportion of the pigment/binder mixture. It was determined that when combining black pigments with *tempera grassa* or with casein, the adhesion of the deposited layer is higher, thus the degree of reflection on sample is higher, having as result

difficulties in "reading" (or cleaning) of the substrate. The experimental models were made in such a way as to simulate a real scenario in which usual painting pigments (either in tempera or oil) were covered with black adherent deposits of diverse origins, thus a complex analysis approach is necessary, without sampling.

The first step in the chain of analyses consisted in the non-contact, non-invasive imagistic investigation using HSI. The hyperspectral images obtained at three wavelengths: 950 nm, 1600 nm and 2200 nm are presented in Figs. 8-10.

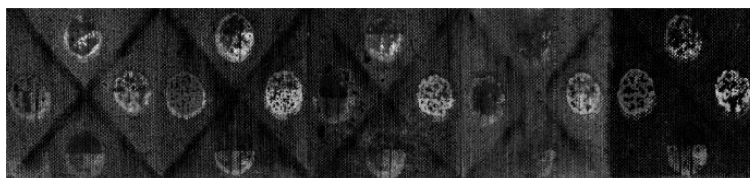*Fig. 8. HS image of Row 5 (tempera grassa) - 950 nm*

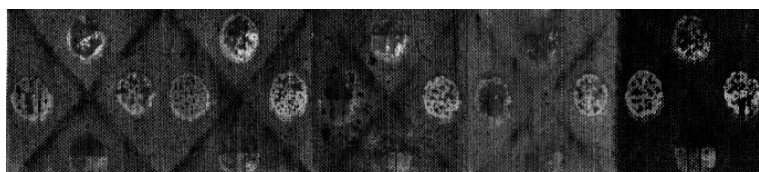*Fig. 9. HS image of Row 5 (tempera grassa) - 1600 nm*

Fig. 10. HS image of Row 5 (tempera grassa) - 2200 nm

By combining the images obtained at different wavelengths we can obtain false colour images that highlight the distribution of the selected pixels on the investigated object, as shown in Fig. 11 where the discrimination of the pigments' layers can be observed.

Fig. 11. HS image – false colour infrared mode (FCIR) composed of 950 nm, 1600 nm and 2200 nm wavelengths

Guided by the HSI, a detailed stratigraphic analysis was pursued using LIBS and Raman spectroscopy, for specific areas of interest. This approach helped reveal the stratigraphic elemental composition at both atomic and molecular levels. By employing LIBS, which efficiently vaporizes a minuscule quantity of material - typically in the micro-grams range - we were able to create a localized plasma plume that facilitates the subsequent analysis through Raman spectroscopy. LIBS point analysis were made on several areas specific to each pigment on series of 5 pulses, single pulse mode.

Table 2. Stratigraphic display of the main chemical elements identified by LIBS on Row 5 (tempera grassa)

Pigment area	Main chemical elements identified
Prussian blue	Pulse 1: Ca, Na, **C** Pulse 2: Ca, Na, **Fe** Pulse 3: Ca, Na, **Fe** Pulse 4: Ca, Na, **Fe**, Pulse 5: Ca, **Ti**, Fe, Na, K, H
Vermilion	Pulse 1: Ca, Na, **C** Pulse 2: Ca, Na, **Hg** Pulse 3: Ca, Na, **Hg** Pulse 4: Ca, Na, **Hg** Pulse 5: Ca, **Ti**, K, Na, Hg
red iron oxide	Pulse 1: Ca, Na, **C** Pulse 2: Ca, **Fe**, Na, K Pulse 3: Ca, **Fe**, Na, K Pulse 4: C, **Fe**, Ti, Ca, Na, K Pulse 5: **Ti**, Ca, C, K, Fe
green earth	Pulse 1: Ca, Na, C Pulse 2: Ca, Na, **K**, C, **Fe**, N Pulse 3: Ca, Na, **K**, **Fe**, **Mg**, **Al**, **Si** Pulse 4: Ca, **Fe**, Na, **K**, C, Ti, **Si**, **Al**, **Mg** Pulse 5: Ca, **Ti**, Fe, Al, Na, Li, K, C

Table 2 presents the stratigraphy disposition of the main elements detected for Row 5, based on spectral relative abundancy. The elements characteristic to each layer are bolded for a better visualization of the stratigraphy. It can be observed that carbon (C) is detected mainly in the first pulses, fact that denotes that 2nd pulse reaches the pigment layer, subsequently appearing chemical elements specific to each pigment: iron (Fe), mercury (Hg), potassium (K), aluminium (Al), silicon (Si), magnesium (Mg). As it can be observed, the in 5th pulse titanium (Ti) appears, along many minority elements, sign that the substrate has been reached. Calcium (Ca) and sodium (Na) are elements present in all the spectra and they can be related to the binders, but also, when phosphorus (P) appears, Ca and C can be correlated to ivory black pigment.

Raman analyses offered similar results for most of the areas. The black pigments (black iron oxide, smoke black, charcoal black, ivory black and graphite) applied in 3 layers, blocked the underlying pigments to different extents, yet the areas pre-cleaned by laser ablation showed an increase in the signal.

In the case of the green and blue pictorial layers, as it can be observed in Fig. 12, Raman detected the pigments' characteristic bands: 278 cm^{-1}, 406 cm^{-1}, 1264 cm^{-1}, 1558 cm^{-1} attributed to the green earth pigment [70], and 479 cm^{-1}, 1032 cm^{-1}, 2127 cm^{-1} associated to the Prussian blue pigment [71,72]. As for the red areas (see Fig. 12), the 585 cm^{-1} band can be attributed to red ochre [73], but several other bands were identified that can be related to: titan dioxide (TiO$_2$) - 449 cm^{-1}, amorphous carbon - 1320 cm^{-1} and 1576 cm^{-1}, and possible lipids at 1434 cm^{-1} [9,74,75]. The situation was similar in the case of vermillion, where besides the characteristic 268 cm^{-1} band, amorphous carbon band appears, as a remain from the ablated layers (1272 cm^{-1}) [70,76-78].

This sequential application of LIBS and Raman techniques not only enhances our understanding of the elemental distribution within the pictorial layers, but also provides valuable insights into the molecular characteristics of the materials present. Through this integrated methodology, we can achieve a more comprehensive characterization of the specific features, ultimately contributing to a deeper understanding of the spatial and compositional complexities of the studied cultural heritage objects.
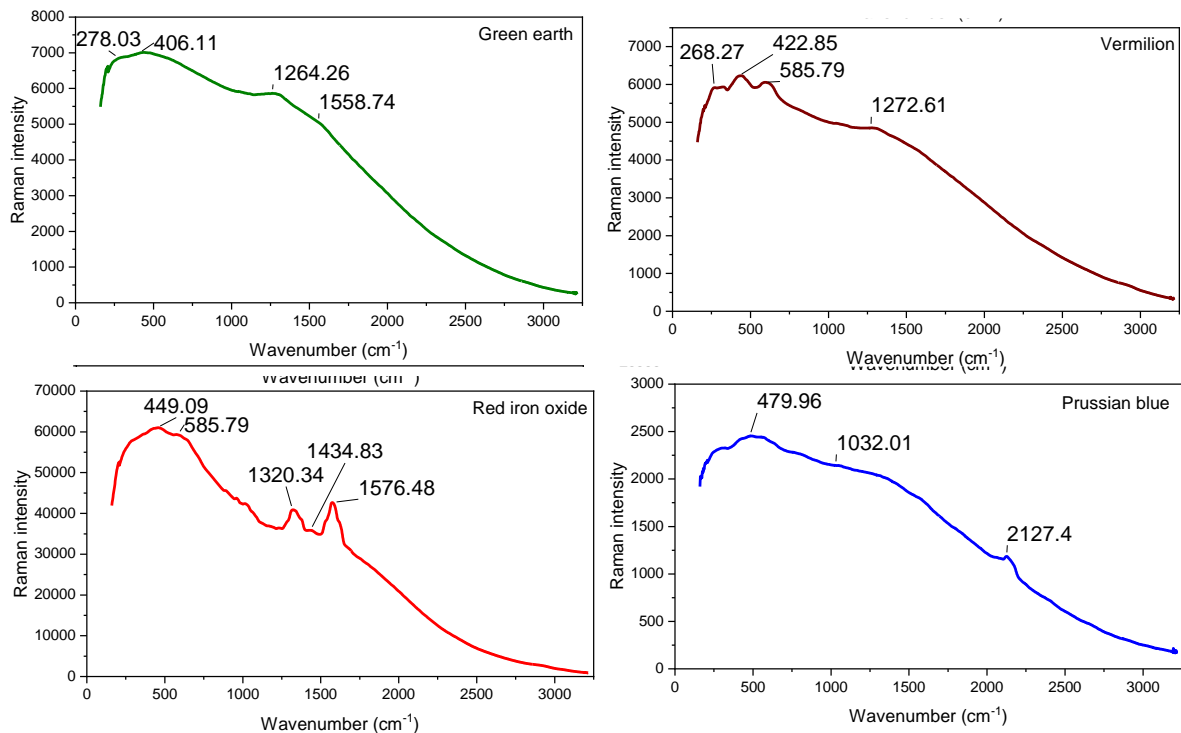
Fig. 12. Raman spectra obtained for laser cleaned areas (color online)

5. Conclusions

Each of the three optoelectronic methods (LIBS, Raman and HSI) yields strong results for specific material categories within distinct spectral domains. When combined, they provide a complex 3D analytical package, offering an effective remote solution for cultural heritage applications, particularly suited to polychrome, multi-layered objects. The convergence of hyperspectral imaging, Raman spectroscopy, and LIBS represents a significant advancement in heritage analysis. By leveraging the strengths of each technique, researchers can construct a comprehensive profile of heritage objects that encompasses material composition, structural integrity, and historical context. The remote investigation and characterization of hidden layers in polychrome surfaces will offer invaluable insights for conservers, restorers, curators, art evaluators, art historians, and archaeologists. This approach delivers detailed information on degradation mechanisms, hidden defects, hidden or concealed underlayers, overpainting, past restorations, the artist's painting technique, and the validation or authentication of both contemporary and historical materials, used in artworks. This multi-dimensional approach not only enriches our understanding of cultural artefacts but also underscores the importance of interdisciplinary collaboration in the preservation of our shared heritage.

By synchronizing these techniques, researchers can achieve a more holistic view of heritage objects:

• *complementary data:* the combination of spectral data from hyperspectral imaging, molecular insights from Raman spectroscopy, and stratigraphic elemental analysis from LIBS allows for a multi-dimensional understanding of materials.

• *targeted conservation strategies*: the integration enables targeted conservation efforts by revealing how different materials interact and degrade over time, informing preservation methods.

• *enhanced research opportunities*: this integrated approach opens new avenues for research, allowing for in-depth studies of the historical, artistic, and technological contexts of artefacts.

Future developments may include the refinement of data processing algorithms to further enhance the real-time analysis capabilities and the potential for automation in data acquisition. Moreover, expanding the application of this method to a broader range of materials - such as textiles, and ceramics - could unlock even more insights into our cultural heritage.

References

[1] H. F. Grahn, P. Geladi, Techniques and Applications of Hyperspectral Image Analysis, Wiley, 2007.
[2] C. I. Chang, Advances in Hyperspectral Image

Processing Techniques, Wiley, 2022.

[3] L. Wang, C. Zhao, Hyperspectral Image Processing, Springer, 2015.

[4] J. M. Amigo, Data Handling in Science and Technology, Elsevier, 2020.

[5] C. Cucci, A. Casini, Data Handling in Science and Technology, Elsevier, 2020.

[6] M. R. López-Ramírez, N. Navas, L. R. Rodríguez-Simón, J. C. Otero, E. Manzano, Analytical Methods **7**, 1499 (2015).

[7] C. Brooke, H. Edwards, P. Vandenabeele, S. Lycke, M. Pepper, Heritage **3**(4), 1148 (2020).

[8] P. Mazzoleni, G. Barone, S. Raneri, E. Aquilia, D. Bersani, R. Cirrincione, Plinius 42, 112 (2016).

[9] M. C. Caggiani, A. Cosentino, A. Mangone, Microchemical Journal 129, 123 (2016).

[10] C. B. Lauridsen, J. Sanyova, K. P. Simonsen, Spectrochim Acta Part A: Molecular and Biomolecular Spectroscopy **150**, 54 (2015).

[11] S. Bottura-Scardina, P. Vandenabeele, C. Miguel, A. Candeias, Journal of Raman Spectroscopy **54**, 1303 (2023).

[12] K. M. E. Hamouda, N. M. N. El Hadidi, S. A. M. Hamed, M. S. Abdel-Aziz, Egyptian Journal of Chemistry **66**(13), 117 (2023).

[13] R. Noll, Laser-Induced Breakdown Spectroscopy: Fundamentals and Applications, Springer, 2012.

[14] S. Siano, J. Agresti, The Encyclopedia of Archaeological Sciences, Wiley, 2018.

[15] J. P. Singh, S. N. Thakur, Laser-Induced Breakdown Spectroscopy, Elsevier, 2007.

[16] A. W. Miziolek, V. Palleschi, I. Schechter, Laser Induced Breakdown Spectroscopy (LIBS): Fundamentals and Applications, Cambridge University Press, 2006.

[17] D. A. Cremers, L. J. Radziemski, Handbook of Laser-Induced Breakdown Spectroscopy, Wiley, 2013.

[18] G. Galbács, Analytical and Bioanalytical Chemistry **407**, 7537 (2015).

[19] G. Galbács, Laser-Induced Breakdown Spectroscopy in Biological, Forensic and Materials Sciences, Springer, 2022.

[20] L. Radziemski, D. Cremers, Spectrochim Acta Part B: Atomic Spectroscopy **87**, 3 (2013).

[21] D. Anglos, Applied Spectroscopy **55**(6), 186A (2001).

[22] K. Müller, H. Stege, Archaeometry **45**(3), 421 (2003).

[23] R. Gaudiuso, M. Dell'Aglio, O. de Pascale, G. S. Senesi, A. de Giacomo, Sensors **10**(8), 7434 (2010).

[24] L. Ghervase, I. M. Cortea, Chemosensors **11**(2), 100 (2023).

[25] S. M. Angel, N. R. Gomer, S. K. Sharma, C. McKay, N. Ames, Applied Spectroscopy **66**(2), 137 (2012).

[26] I. M. Cortea, L. Ghervase, L. Ratoiu, M. Dinu, R. Radvan, Heritage Science **8**, 55 (2020).

[27] T. E. Acosta-Maeda, A. K. Misra, L. G. Muzangwa, G. Berlanga, D. Muchow, J. Porter, S. K. Sharma, Applied Optics **55**(36), 10283 (2016).

[28] S. K. Sharma, Spectrochimica Acta Part A: Molecular

and Biomolecular Spectroscopy **68**(4), 1008 (2007).

[29] S. Wallin, A. Pettersson, H. Östmark, A. Hobro, Analytical and Bioanalytical Chemistry **395**, 259 (2009).

[30] J. H. Hooijschuur, I. E. Iping Petterson, G. R. Davies, C. Gooijer, F. Ariese, Journal of Raman Spectroscopy **44**, 1540 (2013).

[31] S. Legnaioli, B. Campanella, F. Poggialini, S. Pagnotta, M. A. Harith, Z. A. Abdel-Salam, V. Palleschi, Analytical Methods **12**, 1014 (2020).

[32] L. Jolivet, M. Leprince, S. Moncayo, L. Sorbier, C. P. Lienemann, V. Motto-Ros, Spectrochimica Acta Part B: Atomic Spectroscopy **151**, 41 (2019).

[33] G. S. Senesi, R. S. Harmon, R. R. Hark, Spectrochimica Acta Part B: Atomic Spectroscopy **175**, 106031 (2021).

[34] A. Giakoumaki, I. Osticioli, D. Anglos, Applied Physics A **83**, 537 (2006).

[35] B. J. Marquardt, D. N. Stratis, D. A. Cremers, S. M. Angel, Applied Spectroscopy **52**(9), 1148 (1998).

[36] R. C. Wiens, S. K. Sharma, J. Thompson, A. Misra, P. G. Lucey, Spectrochimica Acta Part A: Molecular and Biomolecular Spectroscopy **61**(10), 2324 (2005).

[37] S. K. Sharma, P. G. Lucey, M. Ghosh, H. W. Hubble, K. A. Horton, Spectrochimica Acta Part A: Molecular and Biomolecular Spectroscopy **59**(10), 2391 (2003).

[38] M. Hoehse, D. Mory, S. Florek, F. Weritz, I. Gornushkin, U. Panne, Spectrochimica Acta Part B: Atomic Spectroscopy **64**(11), 1219 (2009).

[39] D. W. Hahn, N. Omenetto, Applied Spectroscopy **66**(4), 347 (2012).

[40] S. Shin, I. J. Doh, K. Okeyo, E. Bae, J. P. Robinson, B. Rajwa, Molecules **28**(16), 6087 (2023).

[41] P. Westlake, P. Siozos, A. Philippidis, C. Apostolaki, B. Derham, A. Telixi, V. Perdikatsis, R. Jones, D. Anglos, Analytical and Bioanalytical Chemistry **402**(4), 1431 (2012).

[42] F. Matroodi, S. H. Tavassoli, Applied Optics **54**(3), 400 (2015).

[43] J. Moros, J. A. Lorenzo, P. Lucena, L. M. Tobaria, J. J. Laserna, Analytic Chemistry **85**(2), 640 (2010).

[44] S. M. Clegg, R. Wiens, A. K. Misra, S. K. Sharma, V. Lambert, S. Bender, R. Newell, K. Nowak-Lovato, S. Smrekar, M. Darby Dyar, S. Maurice, Applied Spectroscopy **68**(9), 925 (2015).

[45] J. Moros, J. A. Lorenzo, J. J. Laserna, Analytical and Bioanalytical Chemistry **400**, 3353 (2011).

[46] I. M. Cortea, L. Ghervase, L. Ratoiu, O. Țentea, M. Dinu, Heritage **7**(9), 5268 (2024).

[47] Y. Li, M. A. Suzuki, C. S. Cheung, S. Kogou, H. Liang, SPIE Proceedings **11784**, 11784 (2021).

[48] R. Bruder, V. Detalle, C. Coupry, Journal of Raman Spectroscopy **38**(7), 909 (2007).

[49] G. Bazalgette Courrèges-Lacoste, B. Ahlers, F. R. Pérez, Spectrochimica Acta Part A: Molecular and Biomolecular Spectroscopy 68(4), 1023 (2007).

[50] R. Radvan, L. Ratoiu, I. M. Cortea, A. Chelmus, L. Angheluta, D. Marinescu, Proceedings - International Conference on Developments in

ESystems Engineering, DeSE. 117 (2019).

[51] A. A. Gowen, Y. Feng, E. Gaston, V. Valdramidis, Talanta **137**, 43 (2015).

[52] M. Picollo, C. Cucci, A. Casini, L. Stefani, Sensors **20**(10), 2843 (2020).

[53] G. Elmasry, D. W. Sun, P. Allen, Journal of Food Engineering **117**(2), 235 (2013).

[54] J. H. Cheng, D. W. Sun, LWT - Food Science and Technology **62**(2), 1060 (2015).

[55] G. ElMasry, M. Kamruzzaman, D. W. Sun, P. Allen, Critical Reviews in Food Science and Nutrition **52**(11), 999 (2012).

[56] M. Dinu, I. M. Cortea, L. Ghervase, M. C. Stancu, I. Mohanu, N. Cristea, J. Optoelectron. Adv. M. **22**(5-6), 303 (2020).

[57] U. Pacher, M. Dinu, T. O. Nagy, R. Radvan, W. Kautek, Spectrochimica Acta Part B: Atomic Spectroscopy **146**, 36 (2018).

[58] A. Kudelski, Talanta **76**(1), 1 (2008).

[59] M. J. Pelletier, Applied Spectroscopy **57**(1), 20A (2003).

[60] M. Simileanu, R. Radvan, J. Optoelectron. Adv. M. **14**(11-12), 1066 (2012).

[61] T. A. Labutin, V. N. Lednev, A. A. Ilyin, A. M. Popov, Journal of Analytical Atomic Spectrometry **31**(1), 90 (2016).

[62] V. Sturm, R. Fleige, M. de Kanter, R. Leitner, K. Pilz, D. Fischer, G. Hubmer, R. Noll, Analytical Chemistry **86**(19), 2014.

[63] K. A. Antonio, Z. D. Schultz, Analytical Chemistry **86**(1), 30 (2014).

[64] G. Hubmer, R. Kitzberger, K. Mörwald, Analytical and Bioanalytical Chemistry **385**, 219 (2006).

[65] Y. Liu, S. Zhao, X. Gao, S. Fu, C. Song, Y. Dou, S. Song, C. Qi, J. Lin, RSC Advances **12**(53), 34520 (2022).

[66] L. Ravikanth, C. B. Singh, D. S. Jayas, N. D. G. White, Biosystems Engineering **135**, 73 (2016).

[67] V. Ljubić Tobisch, I. M. Cortea, L. Ratoiu, R. Radvan, W. Kautek, Microchemical Journal **152**, 104320 (2020).

[68] M. Dinu, L. C. Ratoiu, C. Călin, G. Călin, Buildings **13**(2), 321 (2023).

[69] R. Radvan, M. Dinu, L. C. Ratoiu, M. C. Stancu, Romanian Journal of Physics **68**, 905 (2023).

[70] A. Dal Fovo, L. Sepiacci, S. Innocenti, J. Striova, R. Fontana, Journal of Cultural Heritage **66**, 229 (2024).

[71] M. Ricci, F. Sebastiani, M. Becucci, M. Rogozny, V. Parfenov, Spectroscopy Journal **1**(3), 121 (2023).

[72] M. Corradini, L. de Ferri, G. Pojana, Journal of Raman Spectroscopy **52**(1), 35 (2021).

[73] D. Parras, P. Vandenabeele, A. Sánchez, M. Montejo, L. Moens, N. Ramos, Journal of Raman Spectroscopy **41**, 68 (2010).

[74] H. G. M. Edwards, D. W. Farwell, C. J. Brooke, Analytical and Bioanalytical Chemistry **383**, 312 (2005).

[75] R. Galli, M. Meinhardt, E. Koch, G. Schackert, G. Steiner, M. Kirsch, O. Uckermann, Frontiers in Oncology **9**, 2019.

[76] M. A. García-Bucio, E. Casanova-González, J. L. Ruvalcaba-Sil, E. Arroyo-Lemus, A. Mitrani-Viggiano, Philosophical Transactions of the Royal Society A: Mathematical, Physical and Engineering Sciences **374**, 20160051 (2016).

[77] H. H. Marey Mahmoud, Heritage Science **2**, 18 (2014).

[78] J. M. Chalmers, P. R. Griffiths, Handbook of Vibrational Spectroscopy, Wiley, 2002.

_____

*Corresponding author: monica.dinu@inoe.ro